

This discussion paper is/has been under review for the journal The Cryosphere (TC).  
Please refer to the corresponding final paper in TC if available.

# Permafrost and surface energy balance of a polygonal tundra site in Northern Siberia – Part 2: Winter

M. Langer, S. Westermann, S. Muster, K. Piel, and J. Boike

Alfred-Wegener-Institute for Polar and Marine Research, Telegrafenberg A43,  
14473 Potsdam, Germany

Received: 5 August 2010 – Accepted: 12 August 2010 – Published: 25 August 2010

Correspondence to: M. Langer (moritz.langer@awi.de)

Published by Copernicus Publications on behalf of the European Geosciences Union.

TCD

4, 1391–1431, 2010

## Permafrost and surface energy balance in Northern Siberia – Part 2

M. Langer et al.

Title Page

Abstract

Introduction

Conclusions

References

Tables

Figures

⏪

⏩

◀

▶

Back

Close

Full Screen / Esc

Printer-friendly Version

Interactive Discussion

## Abstract

Permafrost is largely determined by the surface energy balance. Its vulnerability to degradation due to climate warming depends on complex soil-atmosphere interactions. This article is the second part of a comprehensive surface energy balance study at a polygonal tundra site in Northern Siberia. It comprises two consecutive winter periods from October 2007 to May 2008 and from October 2008 to January 2009. The surface energy balance is obtained by independent measurements of the radiation budget, the sensible heat flux and the ground heat flux, whereas the latent heat flux is inferred from measurements of the atmospheric turbulence characteristics and a model approach. The measurements reveal that the long-wave radiation is the dominant factor in the surface energy balance. The radiative losses are balanced to about 60% by the ground heat flux and almost 40% by the sensible heat fluxes, whereas the contribution of the latent heat flux is found to be relatively small. The main controlling factors of the surface energy budget are the snow cover, the cloudiness and the soil temperature gradient. Significant spatial differences in the surface energy balance are observed between the tundra soils and a small pond. The heat flux released from the subsurface heat storage is by a factor of two increased at the freezing pond during the entire winter period, whereas differences in the radiation budget are only observed at the end of winter. Inter-annual differences in the surface energy balance are related to differences in snow depth, which substantially affect the temperature evolution at the investigated pond. The obtained results demonstrate the importance of the ground heat flux for the soil-atmosphere energy exchange and reveal high spatial and temporal variabilities in the subsurface heat budget during winter.

## 1 Introduction

Numerous studies based on climate models revealed that the large-scale atmospheric conditions are greatly impacted by the heat and moisture turnover at the

TCD

4, 1391–1431, 2010

## Permafrost and surface energy balance in Northern Siberia – Part 2

M. Langer et al.

Title Page

Abstract

Introduction

Conclusions

References

Tables

Figures

⏪

⏩

◀

▶

Back

Close

Full Screen / Esc

Printer-friendly Version

Interactive Discussion



surface-atmosphere interface (e.g. Viterbo et al., 1999; Delire et al., 2002; Pitman, 2003; Rinke et al., 2008). Recent studies also showed that the most pronounced arctic warming occurs during the winter and early spring period (Moritz et al., 2002; Johannessen et al., 2004). According to model predictions, it is expected that the significant arctic warming during the last decades (e.g. Overpeck et al., 1997; Comiso, 2003; Hinzman et al., 2005; Tape et al., 2006; Turner et al., 2007; Overland et al., 2008) is accelerated due to positive feedback mechanisms, such as a shrinking sea-ice cover and increased cloudiness (e.g. Holland and Bitz, 2003; Kaplan et al., 2003; Vavrus, 2004).

The winter time surface energy balance of the Arctic constitutes an essential factor in the regional climate system, since it affects the atmospheric heat budget due to sensible, latent and radiative energy exchange with the surface over a long-lasting period. Hence, for the evaluation and the development of large-scale model parameterizations, energy balance studies are an indispensable tool. In the Arctic, only few comprehensive energy balance studies exist within this large geographical area, especially for the winter period. The importance of the winter surface energy balance on the thermal state of the permafrost has been most recently demonstrated by Westermann et al. (2009) for a site on Svalbard: here, the snow surface temperature is largely controlled by the long-wave radiation balance, which in conjunction with the evolution of the snow cover and more complex processes, such as wintertime rain events, determines the thermal regime of the ground. Osterkamp (2005) reported that the winter and spring warming essentially affects the heat budget of permafrost soils.

Energy balance studies give insight into the processes, which are relevant for both the permafrost and the atmospheric heat budget. This is especially important for the development of new model schemes, which aim to incorporate permafrost due to its high carbon stock and its potential feedback to climate change. Recent effort in global permafrost modeling has already been initiated (e.g. Stendel and Christensen, 2002; Lawrence and Slater, 2005; Nicolsky et al., 2007; Lawrence et al., 2008). However, the accuracy of these models depend on the realistic representation of the

## Permafrost and surface energy balance in Northern Siberia – Part 2

M. Langer et al.

Title Page

Abstract

Introduction

Conclusions

References

Tables

Figures

⏪

⏩

◀

▶

Back

Close

Full Screen / Esc

Printer-friendly Version

Interactive Discussion

ground-atmosphere energy exchange processes, which are determined by parameterizations of the local surface and subsurface properties (e.g. roughness length, soil heat conductivity, snow cover characteristics).

This study is the second part of a comprehensive investigation on the annual surface energy balance at a wet tundra site in Northern Siberia. The results of the first part of this study (Langer et al., 2010) revealed that the sensitivity of the permafrost heat budget towards variations in radiation balance and turbulent heat fluxes is highest at the beginning and end of the summer thaw cycle. Furthermore, the permafrost heat budget appears to be less sensitive to surface energy balance variations during the high summer period. In this second paper, we focus on the surface energy balance during the winter periods from 1 October 2007, until 30 March 2008, and 1 October 2008, until 30 January 2009. We aim to achieve (i) the identification of the controlling and limiting factors of the surface energy balance, (ii) the evaluation of the seasonal and inter-annual variability of the energy balance components and (iii) the detection and evaluation of spatial differences of the surface energy balance by spatially distributed measurements. The results are discussed with respect to larger-scale modeling of the arctic boundary layer and the permafrost.

## 2 Study site

The study site is located at the southern part of the Lena River Delta on Samoylov Island (72°22' N; 126°30' E) (Fig. 1). The regional climate is arctic-continental with a mean annual air temperature (MAAT) of about -13 °C, a pronounced annual temperature amplitude of about 60 °C and a total annual precipitation around 250 mm (Boike et al., 2008). Snow fall and soil refreezing begins towards the end of September. The winter period is characterized by the polar night, which lasts from mid of November until end of January. The climate and synoptic conditions during the winter are largely determined by the Siberian High, which causes air temperatures to fall frequently below -45 °C. The high pressure system is often disturbed by the influx of cyclones with high

### Permafrost and surface energy balance in Northern Siberia – Part 2

M. Langer et al.

Title Page

Abstract

Introduction

Conclusions

References

Tables

Figures

⏪

⏩

◀

▶

Back

Close

Full Screen / Esc

Printer-friendly Version

Interactive Discussion



Discussion Paper | Discussion Paper | Discussion Paper | Discussion Paper | Discussion Paper

intensity and short lifetime (Zhang et al., 2004). The continental climate conditions are also reflected in the thermal regime of the soil, which is characterized by continuous permafrost reaching depths of 500–600 m (Grigoriev, 1960). At the depth of the zero annual amplitude ( $\approx 15$  m) the soil temperature is about  $-10^\circ\text{C}$ . During the summer months, the maximum thaw depth ranges from 0.4–0.5 m. The tundra surface is highly fractionated due to polygonal structures, which are typically 50–100 m<sup>2</sup> large. The rims of these polygons are elevated by about 0.2 to 0.5 m compared to the centers, which consist of water-saturated peat soils or constitute ponds, which frequently occur at the study site. During the winter period, the tundra soils are covered by a shallow snow layer, which typically features depths of less than 0.5 m at the depressed centers and only a few centimeters at the elevated rims.

### 3 Methods

For the evaluation of the surface energy balance and the quantification of spatial variabilities at the study site we distinguish between two basic landscape features during the winter period: the snow covered tundra soils and freezing or frozen water bodies. The surface energy balance of the snow covered tundra soils (referred to as tundra site) is measured as a spatial average including polygonal centers and rims (compare Sect. 2). Components of the energy balance (net radiation, subsurface heat flux) of water bodies are exemplified at a polygonal pond (referred to as pond site). The energy balance equation for the tundra site is written as

$$Q_{\text{net}} = Q_{\text{H}} + Q_{\text{E}} + Q_{\text{G}} + C \quad (1)$$

where  $Q_{\text{net}}$  is the net radiation,  $Q_{\text{H}}$  the turbulent sensible heat flux,  $Q_{\text{E}}$  the turbulent latent heat flux,  $Q_{\text{G}}$  the subsurface (ground or snow) heat flux and  $C$  is the residual of the energy balance, which accounts for inaccuracies of measurement. The pond, at which the net radiation  $Q_{\text{net,p}}$  and the subsurface heat flux  $Q_{\text{G,p}}$  are measured, features a depth of about 0.8 m and a water volume of about 150 m<sup>3</sup>. The basic concepts

## Permafrost and surface energy balance in Northern Siberia – Part 2

M. Langer et al.

Title Page

Abstract

Introduction

Conclusions

References

Tables

Figures

⏪

⏩

◀

▶

Back

Close

Full Screen / Esc

Printer-friendly Version

Interactive Discussion



of the measurements and the data analysis applied in the present study are already described in the first part of this study (Langer et al., 2010). The applied methods are re-summarized briefly, while new methods and additional measurements are described in more detail in the following sections.

### 3.1 Radiation balance

The net radiation at the tundra  $Q_{\text{net}}$  and pond sites  $Q_{\text{net,p}}$  are measured with net radiations sensors (NR-Lite, Kipp and Zonen, The Netherlands). The net radiation sensor at the tundra site is not available in the second winter period (2008–2009), but we apply a four-component radiation sensor (CNR1, Kipp and Zonen, The Netherlands) to calculate the net radiation. The outgoing thermal radiation at the tundra site is measured separately by a long-wave radiation sensor in winter 2007–2008 (CG1, Kipp and Zonen, The Netherlands) and calculated from infrared surface temperature sensors (IRTS-P, Apogee Instruments, USA) in winter 2008–2009 using Stefan-Boltzmann law (compare Langer et al., 2010). For this calculation, we assume the surface emissivity of the snow cover to be 0.98 according to commonly used values (Rees, 1993).

### 3.2 Turbulent heat fluxes

Measurements of the sensible heat flux  $Q_{\text{H}}$  are only available for the tundra site. The flux sources area at the location of the eddy covariance system is characterized to about 95% by tundra soils, according to a foot print analyses (Langer et al., 2010). The eddy covariance setup is reduced to the 3-D sonic anemometer (C-SAT, Campbell Scientific, USA) during the observation period from 1 October to 30 March. The reduced measurement setup only permits the detection of the momentum flux  $u_*^2$  and the buoyancy flux  $Q_{\text{HB}}$ , which in principle must be corrected according to the flux of water vapor to obtain the true sensible heat flux  $Q_{\text{H}}$  (Schotanus et al., 1983). Due to the extremely cold air temperatures, we assume the flux of water vapor to be very small during winter, so that the difference between the buoyancy and sensible heat flux is small. Hence,

## Permafrost and surface energy balance in Northern Siberia – Part 2

M. Langer et al.

Title Page

Abstract

Introduction

Conclusions

References

Tables

Figures

⏪

⏩

◀

▶

Back

Close

Full Screen / Esc

Printer-friendly Version

Interactive Discussion



we accept the buoyancy flux to be a good approximation of the real sensible heat flux during the winter period. According to a quality check and the exclusion of the lee wind sector (263° to 277°), about 18% of the flux measurements must be discarded. From the stability parameter  $\zeta$ , the atmospheric stratification can be inferred, with  $\zeta \approx 0$  for a well mixed or neutrally stratified atmosphere,  $\zeta > 0$  for stable and  $\zeta < 0$  for unstable atmospheric stratifications.

The latent heat flux  $Q_E$  at the tundra site is modeled by an approach similar to the one used in the first part of this study (Langer et al., 2010). The model uses the often applied parametrization introduced by Högström (1988) and is based on available eddy-covariance measurements of the momentum flux  $u_*^2$  and the buoyancy flux  $Q_{HB}$ , from which a turbulent transport coefficient can be inferred (compare Langer et al., 2010). In addition, the model requires measurements of relative humidity and surface temperature for calculating the near-surface gradient of the specific humidity. During winter 2007–2008, we rely on measurements of relative humidity from the standard climate station in the vicinity of the eddy covariance system. During winter 2008–2009, the relative humidity is estimated to be in the range of  $(70 \pm 5)\%$  according to the measurements of the previous year.

### 3.3 Subsurface heat fluxes

Subsurfaces heat fluxes are calculated for a tundra site ( $Q_G$ ) and a thermokarst pond ( $Q_{G,p}$ ). The subsurface heat flux is the heat flux across the surface, which depending on the applied measurement method is defined as the soil, the snow, or the lake ice surface. For the heat flux calculations, we apply the calorimetric and the conductive method (compare Langer et al., 2010).

#### 3.3.1 The calorimetric method

The calorimetric method calculates the ground heat flux based on changes in the internal energy of a soil column using measurements of the soil temperature and liquid

## Permafrost and surface energy balance in Northern Siberia – Part 2

M. Langer et al.

Title Page

Abstract

Introduction

Conclusions

References

Tables

Figures

⏪

⏩

◀

▶

Back

Close

Full Screen / Esc

Printer-friendly Version

Interactive Discussion



water content  $\theta_w$ . This method is used for evaluating averages of the ground heat flux over periods longer than a few days. Due to the measurements of temperature and liquid water content, it is possible to distinguish sensible and latent heat storage, which we express as energy fluxes  $Q_{G,sensible}$  and  $Q_{G,latent}$ . Note, that the heat storage in the shallow snow layer becomes negligible for long-term averages, so that temperature profiles in the snow pack are not required. During winter 2007–2008, soil temperatures are available from a 26 m borehole and a thermistor profile in the active layer (CA I) (Fig. 2). The liquid water content  $\theta_w$  is measured in the active layer by Time-Domain-Reflectometry (TDR) probes (compare Langer et al., 2010). Since the deep borehole and the TDR probes are not available during winter 2008–2009 (CA II), we rely on a shallow borehole of 4 m depth and a parametrization of the liquid water content in dependence of the soil temperature. This so-called freezing characteristic is inferred by fitting a polynomial function to measurements of water content and temperature of the previous year (Fig. 3). Since the calorimetric method requires measurements down to a depth of zero temperature change in the concerned averaging period, heat fluxes below 4 m are required. We therefore calculate the heat flux through the lower boundary of the temperature profile by using the conductive method (compare Langer et al., 2010). Soil heat capacities, thermal diffusivity and heat conductivity of frozen tundra soils are evaluated similar to the summer time values (Table 6).

### 3.3.2 The conductive method

The conductive method calculates the heat flux across a layer by solving the differential equation of conductive heat transport (compare Langer et al., 2010). In addition, the conductive method involves the determination of the thermal diffusivity of snow or soil, which are presented in Table 6. The conductive method is applied for both calculations of the subsurface heat flux at (a) the tundra site and (b) the thermokarst pond.

- (a) For the tundra site, this method is applied for calculating heat fluxes with hourly resolution. These high resolution heat fluxes are only obtained at polygonal

## Permafrost and surface energy balance in Northern Siberia – Part 2

M. Langer et al.

Title Page

Abstract

Introduction

Conclusions

References

Tables

Figures

⏪

⏩

◀

▶

Back

Close

Full Screen / Esc

Printer-friendly Version

Interactive Discussion





**Permafrost and  
surface energy  
balance in Northern  
Siberia – Part 2**

M. Langer et al.

Title Page

Abstract

Introduction

Conclusions

References

Tables

Figures

⏪

⏩

◀

▶

Back

Close

Full Screen / Esc

Printer-friendly Version

Interactive Discussion



ice layer, as soon as it approaches a thickness of 24 cm, which then contains the two uppermost temperature sensors of the profile. We use the conductive method described in Langer et al. (2010) to evaluate the heat flux through the ice cover surface with the known thermal diffusivity and conductivity of ice. The employed values are depicted in Table 6.

### 3.4 Snow cover measurements

We use different methods for the detection of the snow depth. The snow depth is measured with an ultrasonic ranging sensors (SR50, Campbell Scientific, USA) located at the tundra site and at the pond site. During winter 2008–2009, the ultrasonic sensor is not available at the tundra site. Therefore, we infer the snow depth from the snow temperature profile described in Sect. 3.3 using the method of Lewkowicz (2008), who determines the snow depth from a significant temperature decoupling between buried and unburied sensors. The temperature profile provides a vertical resolution of 5 cm. In addition, we use the AMSR-E 5-Day L3 snow water equivalent (SWE) product (Kelly et al., 2004) to obtain a complementary snow cover information in addition to our point measurements. The satellite product is based on passive microwave detection and features a spatial resolution of 25 km. A detailed technical description of the product and the retrieval algorithm is given by Pulliainen and Hallikainen (2001). For tundra surfaces, the accuracy of the SWE product is expected to be in the range of 10%, since the shallow vegetation only marginally affects the snow cover signal (Foster et al., 2005). We selected the closest pixel to the study site, which must be understood as an averages value over a large variety of surface structures.

Moreover, SWE field measurements are conducted during April 2008 and 2009. From these measurements, we calculate the snow heat capacity, which is used for the heat flux calculations. The obtained values are presented in Table 6. The field measurements of the snow density  $\rho_{\text{snow}}$  are further used for the conversion of the AMSR-E dataset from SWE to snow depths.

## 4 Results

In the following, we describe the winter surface energy balance. We divide the observation period into three sections, according to the availability of sunlight. During the first and the last winter sections short wave radiation is still or again present, whereas the middle period is characterized by the absence of sunlight due to polar night conditions.

### 4.1 Early winter (1 October–30 November)

The first winter period lasts from the beginning of October until the end of November, immediately before the beginning of the polar night. The surface energy balance is characterized by a strongly negative radiation budget on the order of  $-20 \text{ W m}^{-2}$ , which is about  $25 \text{ W m}^{-2}$  less compared to the preceding fall season (compare Langer et al., 2010). The short-wave radiation budget is very small ( $\approx 2 \text{ W m}^{-2}$ ) due to the high albedo of the snow cover. The negative radiation budget is largely balanced by the ground heat flux  $Q_G$  ( $-10$  to  $-20 \text{ W m}^{-2}$ ), whereas the sensible heat flux  $Q_H$  shows only a marginal contribution of about  $-5 \text{ W m}^{-2}$ , which is only slightly more negative than during the fall season. The modeled latent heat flux  $Q_E$  is still significantly positive ( $\approx 10 \text{ W m}^{-2}$ ), which agrees with the high values measured in the previous fall period. Similar to the fall period, the energy balance residual  $C$  is considerable, which indicates that some heat flux is not detected.

The general weather conditions are characterized by rapidly declining air temperatures, decreasing sun angles, snow accumulation and the freezing of soil and water bodies. In both years, the air temperatures rapidly fall from about  $0^\circ\text{C}$  at the beginning to  $-20^\circ\text{C}$  at the end of the period. The build-up of a continuous snow cover starts in both winters at the beginning of October. However, we observe significant differences in the evolution of the snow cover at the tundra site. In 2007, the snow cover reaches a depth of about 0.15 m shortly after the first snow fall and remains almost constant until the end of the period. In 2008, the snow cover accumulation is much slower and ends up with a snow depth of about 0.1 m (Fig. 4). An even greater inter-annual variability

## Permafrost and surface energy balance in Northern Siberia – Part 2

M. Langer et al.

Title Page

Abstract

Introduction

Conclusions

References

Tables

Figures

◀

▶

◀

▶

Back

Close

Full Screen / Esc

Printer-friendly Version

Interactive Discussion



the snow depth is observed at the pond site, which in 2007 is covered by about 0.2 m of snow shortly after the first snow fall, whereas in 2008 almost no snow cover is measured until the end of this winter period (Fig. 4). The observed inter-annual differences in snow cover accumulation agree with the satellite observations (AMSR-E) (Fig. 4).

5 The net radiation budget of the first winter period is dominated by the long-wave radiation  $\Delta Q_L$ , which in 2008 is about fifteen times larger than the net short-wave radiation (Table 6, Fig. 5). The incoming long-wave radiation steadily decreases from about  $300 \text{ W m}^{-2}$  to  $180 \text{ W m}^{-2}$ . This general trend is overlain by rapid variations in the range of  $60\text{--}70 \text{ W m}^{-2}$ , which are most likely associated with changes in cloudiness.

10 In frequent situations, the outgoing and the incoming long-wave radiation are in quasi-balance ( $Q_{\text{net}} \approx 0$ ), which is most likely caused by a dense cloud cover. The outgoing long-wave radiation follows the general trend of its incoming counterpart and decreases from about  $315 \text{ W m}^{-2}$  to  $200 \text{ W m}^{-2}$ , which corresponds to a surface temperature cooling from 0 to  $-24^\circ\text{C}$ . The surface temperature of 2008 appears to be slightly increased

15 compared to 2007 (Table 6), which on average amounts to an increased radiative loss on the order of  $5 \text{ W m}^{-2}$  in 2008. The surface temperature follows to a large extent the short-term fluctuations of the incoming long-wave radiation. The observed fluctuations are on the order of  $10^\circ\text{C}$ . The negative net radiation is partly balanced by the sensible heat flux  $Q_H$ , which is negative in both years. In both years, the average values

20 of the sensible heat fluxes are small compared to the ground heat fluxes, but show strong short-term variations on the order of  $30 \text{ W m}^{-2}$ . The observed fluctuations in the sensible heat fluxes largely follow the stepwise variations of the net radiation. Slightly positive sensible heat fluxes, that drag heat from the surface to the atmosphere, are observed occasionally. These events are strictly correlated to high values of down-

25 welling thermal radiation and positive temperature gradients between the surface and the near-surface air temperature. High absolute values of the sensible heat flux are almost always associated with high wind speeds and strong turbulent exchange. The atmospheric stratification is mostly neutral ( $\zeta \approx 0$ ), while stable stratification ( $\zeta > 0$ ) only occur occasionally under clear-sky and calm conditions. Such stable stratifications are

## Permafrost and surface energy balance in Northern Siberia – Part 2

M. Langer et al.

[Title Page](#)[Abstract](#)[Introduction](#)[Conclusions](#)[References](#)[Tables](#)[Figures](#)[⏪](#)[⏩](#)[◀](#)[▶](#)[Back](#)[Close](#)[Full Screen / Esc](#)[Printer-friendly Version](#)[Interactive Discussion](#)

characterized by a very high snow heat flux, which compensates for the reduced sensible heat flux under stable conditions. The largest fraction of the negative radiation budget is balanced by the ground heat flux  $Q_G$ , which is predominately supplied by latent heat of freezing (Table 6). In the inter-annual comparison, the ground heat flux of 2008 is significantly larger than in 2007. This difference corresponds to the lower surface temperatures, the faster snow cover build-up and the slightly increased sensible heat flux of 2007 (Table 6). The observed inter-annual differences in the soil heat fluxes agree with the fact, that the active layer is completely frozen by the end of the early winter period in 2008, but not in 2007.

The most pronounced inter-annual differences in the ground heat budget are observed at the polygonal pond. According to the temperature profile measurements, we can estimate the ice cover thickness to be about 30 cm at the end of the early winter period in 2007. In 2008, the temperature measurements indicate that the water body is completely frozen down to a depth of 85 cm. Assuming an ice density of about  $920 \text{ kg m}^{-3}$ , this amount of ice corresponds to an average heat flux  $Q_{G,p}$  of about  $-12 \text{ W m}^{-2}$  in 2007 and about  $-34 \text{ W m}^{-2}$  in 2008. Note, that these heat fluxes are only estimated according to the amount of frozen water, which does not contain the temperature change of the water body and the ground underneath. Hence, the true ground heat flux at the pond must be even larger. However, in the 2007, the estimated heat flux value at the freezing pond is in a good agreement with the net radiation  $Q_{\text{net},p}$ , which we measure directly at the surface of the water body (Table 6). It is evident, that such an energy balance agreement is not given in 2008, were the pond heat flux releases about  $10 \text{ W m}^{-2}$  more than is lost by radiation. Hence, additional heat transport, such as a positive sensible heat flux, may be involved at the pond surface.

## 4.2 Polar winter (1 December–30 January)

The polar winter section features a highly negative net radiation budget in the range of  $-20$  to  $-25 \text{ W m}^{-2}$ . Due to polar night conditions, the radiation balance is only

### Permafrost and surface energy balance in Northern Siberia – Part 2

M. Langer et al.

Title Page

Abstract

Introduction

Conclusions

References

Tables

Figures



Back

Close

Full Screen / Esc

Printer-friendly Version

Interactive Discussion



determined by thermal radiation. The largest fraction of the radiative loss is balanced by the ground heat flux  $Q_G$ , which is on the order of about  $-15 \text{ W m}^{-2}$ . Compared to early winter, the sensible heat flux  $Q_H$  decreases and is now on the order of  $-10 \text{ W m}^{-2}$ . The latent heat flux  $Q_E$  is significantly lowered and features a value of only  $4 \text{ W m}^{-2}$ .

5 The polar winter section is characterized by the absence of solar radiation during which the air temperatures reach their annual minimum of about  $-44^\circ\text{C}$  in winter 2007–2008 and  $-42^\circ\text{C}$  in winter 2008–2009. During winter 2007–2008, the snow cover remains almost constant featuring a depth of about 15 cm at the tundra surface and about 20 cm at the polygonal pond. A slightly different evolution of the snow cover  
10 is found for 2008–2009, when the snow depth remains between 10 and 15 cm at the tundra surface, whereas almost no snow cover is detected at the pond. For the winter 2007–2008, freezing continues from early winter into the polar night period. While the remaining unfrozen soil layer is already frozen after a few days, the pond remains partially unfrozen until the end of this section (Fig. 4). This delayed freezing process  
15 in 2007–2008 significantly influences the temperature at the bottom of the water body, which is about  $15^\circ\text{C}$  warmer compared to the following year (Fig. 4).

The energy balance of the polar winter section is entirely governed by the long-wave budget  $\Delta Q_L$ , which is significantly negative (Table 6). In both years, the incoming long-wave radiation shows frequent fluctuations according to changes between over-  
20 cast and clear-sky conditions. The measured radiation values vary between 140 and  $240 \text{ W m}^{-2}$ . Conditions of constant incoming radiation typically last between two and three days. The surface temperatures and thus the outgoing thermal radiation show a strong variability in the range of  $-15^\circ\text{C}$  to  $-45^\circ\text{C}$  in both years, which corresponds to emitted radiative fluxes of about  $-150$  and  $-250 \text{ W m}^{-2}$ . The negative radiation budget  
25 is partly balanced by a slightly increased sensible heat flux compared to early winter (Table 6, Fig. 5). The largest fraction of the net radiation is balanced by the ground heat flux  $Q_G$ , which is mainly supplied by the release of sensible heat  $Q_{G,\text{sensible}}$  (Table 6) that originates to about 85% from the first four meters of the soil column. Recalling the inter-annual difference in the ground heat fluxes during the early winter section, the

## Permafrost and surface energy balance in Northern Siberia – Part 2

M. Langer et al.

[Title Page](#)[Abstract](#)[Introduction](#)[Conclusions](#)[References](#)[Tables](#)[Figures](#)[⏪](#)[⏩](#)[◀](#)[▶](#)[Back](#)[Close](#)[Full Screen / Esc](#)[Printer-friendly Version](#)[Interactive Discussion](#)

differences are now reversed. The ground heat flux of 2007 is now higher compared to 2008, which corresponds to a warmer soil in 2007 and therefore to a steeper soil temperature gradient.

An exemplary situation during the transition from the early winter to the polar night in 2007–2008 is depicted in Fig. 6. The example shows the typical stepwise pattern of the long-wave radiation budget, most likely caused by the influence of clouds. These large-scale variations are followed by the course of the sensible heat flux and the ground heat flux, which usually balances the largest fraction of the radiative losses. The turbulent heat flux becomes large ( $Q_H \approx -30 \text{ W m}^{-2}$ ) under clear-sky and windy conditions (wind speed  $\approx 8 \text{ m s}^{-1}$ ), as they occur around 23 November and 4 December. The negative radiation budget is then primarily balanced by the sensible heat flux, which leads to a subsequent surface warming that essentially reduces the snow temperature gradient and thus the ground heat flux (compare Fig. 6). On rare occasions, the net radiation is found to be positive, which can only be associated with the influx of warm air mass that are warmer than the surface and lead to slightly positive sensible heat fluxes (Fig. 6). During one of these situations, we can observe the development of a slightly unstable stratification ( $\zeta < 0$ ) around 25 November (Fig. 6). This situation is due to a precedent long-lasting period of calm conditions featuring stable stratifications and high radiative losses, which most likely cool the atmosphere. The sudden influx of warm air, which is indicated by the rapidly increasing net radiation to positive values heats up the surface. This consequently leads to a positive near-surface temperature gradient and the short-time development of unstable conditions. The unstable stratification breaks down as the net radiation falls back to negative values (Fig. 6).

The largest inter-annual differences in the ground heat budget are again observed at the investigated pond (Table 6), which in 2007–2008 is finally frozen by the end of the polar winter. Similar to the ground heat flux  $Q_G$ , the pond heat fluxes  $Q_{G,p}$  is now higher in 2007–2008 than in 2008–2009. We also observe that in both years the released energy at the pond  $Q_{G,p}$  is larger than the radiative losses  $Q_{\text{net},p}$ , which indicates that amplified turbulent sensible heat fluxes might occur at the surface of the

## Permafrost and surface energy balance in Northern Siberia – Part 2

M. Langer et al.

Title Page

Abstract

Introduction

Conclusions

References

Tables

Figures

⏪

⏩

◀

▶

Back

Close

Full Screen / Esc

Printer-friendly Version

Interactive Discussion

frozen water body similar to the early winter period. Compared to the ground heat flux at the tundra surface  $Q_G$ , the pond heat flux is higher by a factor of about two.

### 4.3 Late winter (1 February–30 March)

The energy balance of the late winter section is still characterized by negative net radiation  $Q_{\text{net}}$  of about  $-15 \text{ W m}^{-2}$ , which is still significantly lower compared to the following spring period, described in the first part of this study. This is due to the fact that the net radiation budget steeply increases during this and the following period. The ground heat flux  $Q_G$  features about  $-5 \text{ W m}^{-2}$  and loses its dominant role in balancing the radiation budget. The largest fraction of radiative losses is now balanced by a further increased sensible heat flux  $Q_H$ , which is on the order of  $-10 \text{ W m}^{-2}$ . The modeled latent heat flux  $Q_E$  remains small at about  $3 \text{ W m}^{-2}$ .

The synoptic conditions are determined by the end of the polar night and increasing air temperatures from about  $-35$  to  $-5^\circ\text{C}$ . The snow depth in 2008 slightly increases of about 5–10 cm and reaches its annual maximum of 25–30 cm.

The average net radiation budget is still negative and reaches values as low as  $-40 \text{ W m}^{-2}$ , while positive fluxes can exceed  $20 \text{ W m}^{-2}$  (Fig. 7). Positive net radiation values frequently occur within a pronounced diurnal cycle towards the end of this period. The upwelling long-wave radiation ranges from 160 and  $300 \text{ W m}^{-2}$ , which corresponds to surface temperatures of  $-40$  and  $-3^\circ\text{C}$ . The sensible heat flux is significantly more negative compared to the polar winter period and balances about 70% of the negative radiation budget, while the ground heat flux loses its dominant role. This corresponds to the evolution of a strong temperature gradient in the atmospheric boundary layer, which frequently exceeds values of  $-3^\circ\text{C}$  with an average gradient of about  $-1^\circ\text{C}$  (Table 6). The sensible heat flux features a diurnal cycle towards the end of the later winter period and ranges from  $-40 \text{ W m}^{-2}$  to  $5 \text{ W m}^{-2}$  (Fig. 7). Positive sensible heat fluxes are usually observed during local noon, when the net radiation is positive due to high values of incoming solar radiation. The atmospheric stratification is essentially neutral during the first half of the late winter section, which corresponds

## Permafrost and surface energy balance in Northern Siberia – Part 2

M. Langer et al.

Title Page

Abstract

Introduction

Conclusions

References

Tables

Figures

⏪

⏩

◀

▶

Back

Close

Full Screen / Esc

Printer-friendly Version

Interactive Discussion



to high wind speeds (Fig. 7). Within the course of the late winter period, the stability parameter  $\zeta$  indicates frequent changes between stable and unstable stratifications (Fig. 7). The ground heat flux is essentially supplied by sensible heat from the deep soil layers. About 85% of the released heat originates from soil cooling down to a depth of 7 m. A more detailed look at the ground heat flux reveals more frequent positive heat fluxes towards the end of the period, which are usually associated with strongly negative sensible heat fluxes (Fig. 7). This indicates that at the end of the entire winter period the initial warming of the ground is mainly supplied by sensible heat fluxes from the atmosphere. These observations are in good agreement with heat fluxes measured in the following spring period, which are described in the first part of this study.

Significant spatial differences of the energy balance are still observed between the polygonal pond and the tundra site. The ground heat flux at the polygonal pond  $Q_{G,p}$  is significantly increased compared to the tundra ground heat flux  $Q_G$ , which corresponds to the more negative radiation budget at the pond  $Q_{net,p}$  (Table 6). This indicates that the polygonal pond most likely features slightly higher surface temperatures. If we assume the surface albedo at the snow covered tundra to be similar to the snow-covered pond, the surface at the pond would be about 1 °C warmer, according to the increased ground heat flux.

#### 4.4 Controlling factors of surface temperature

The surface temperature  $T_{surf}$  is a direct result of the surface energy balance. It is therefore worthwhile to give an insight into its determining factors. We can see in Fig. 8, that the surface temperature variations are primarily determined by the incoming thermal radiation, while other factors, such as wind speed only have a secondary impact. Figure 8 also shows that the impact of wind on the surface temperature is highest during low values of incoming long-wave radiation. This relation is explained by the fact, that the surface cools down strongest under clear-sky conditions when the turbulent heat transport from the atmosphere to the surface is limited by the absence of wind. This describes the typical situation of a near-surface temperature inversion under a stable

## Permafrost and surface energy balance in Northern Siberia – Part 2

M. Langer et al.

Title Page

Abstract

Introduction

Conclusions

References

Tables

Figures



Back

Close

Full Screen / Esc

Printer-friendly Version

Interactive Discussion



atmospheric stratification ( $\zeta > 0$ ), which leads to pronounced surface cooling. However, such conditions are observed only occasionally, since wind-induced turbulent mixing dominates during the polar night (Fig. 8), so that the formation of stable stratifications ( $\zeta > 0$ ) is essentially limited.

## 5 Discussion

### 5.1 The winter time energy balance

According to our measurements, the surface energy balance during winter is predominately characterized by (i) the long-wave radiation budget, (ii) the ground heat flux and (iii) to a minor extent by the atmospheric sensible heat flux. The latent heat flux is found to be small in proportion to the other heat fluxes.

- (i) The radiation budget of the considered winter period is largely determined by the long-wave radiation, as it mostly falls within the polar night, while the high albedo of the snow cover limits the role of the short-wave radiation at the beginning and the end of the period (Table 6). The net long-wave radiation fluctuates strongly between almost zero and highly negative values of up to  $-50 \text{ W m}^{-2}$ . The fluctuations are largely caused by fast changes of the incoming long-wave radiation, which most likely can be attributed to the presence or absence of a cloud cover (Curry et al., 1993; Shupe and Intrieri, 2004). The incoming long-wave radiation is the determining factor for the surface temperature, as it sets the general range within which the surface temperature can adjust depending on the other components of the energy balance (Fig. 8).
- (ii) The ground heat flux is of outstanding importance for the surface energy balance during the winter periods, since it is the main balancing factor of the radiative losses. It originates from both the refreezing of the active layer and the cooling of the soil, with both contributing about 60% to the energy balance. Hereby the

## Permafrost and surface energy balance in Northern Siberia – Part 2

M. Langer et al.

Title Page

Abstract

Introduction

Conclusions

References

Tables

Figures

⏪

⏩

◀

▶

Back

Close

Full Screen / Esc

Printer-friendly Version

Interactive Discussion



**Permafrost and surface energy balance in Northern Siberia – Part 2**

M. Langer et al.

Title Page

Abstract

Introduction

Conclusions

References

Tables

Figures



Back

Close

Full Screen / Esc

Printer-friendly Version

Interactive Discussion



refreezing of the active layer strongly dominates until about the beginning of December. Afterwards the ground heat flux is entirely supplied by soil cooling up to a depth of 15 m. Strong inter-annual differences in the subsurface heat flux are observed particularly during the early winter section (Table 6), with reduced heat fluxes and a delayed refreezing in 2007. This is most likely due to the faster snow cover build up in this year (Fig. 4), related to the low thermal conductivity by a factor of four to eight lower than the thermal conductivity of frozen peat (Table 6). Consequently, the release of heat occurs over a longer period in 2007, while it is more concentrated at the beginning of the winter in 2008. Moreover, profound spatial differences in the subsurface heat fluxes are observed between the tundra soils and the shallow water bodies at which the released heat flux is almost a factor of two higher.

- (iii) While the interplay between the net radiation, the ground heat flux and the sensible heat flux can be complex (Fig. 6), the magnitude of the average sensible heat flux is significantly smaller than the ground heat flux. The highest values of sensible heat fluxes are observed at the end of the winter season. During the entire winter period the observed average sensible heat flux of about  $-8 \text{ W m}^{-2}$  amounts to a cooling of an air column of 1000 m height by about  $30^\circ\text{C}$  over a period of 6 months. This matches the order of magnitude of the observed near-surface temperature cooling, which is also on the order of  $30^\circ\text{C}$  (compare Table 6). In addition, the well mixed boundary layer with predominately neutral stratifications suggests a prominent role of the sensible heat flux for the cooling of the near surface atmosphere. It must be emphasized, that the contribution of the wintertime sensible heat flux to the surface energy balance is by a factor of two smaller than values reported for arctic-oceanic conditions on Svalbard (Westermann et al., 2009), but of similar magnitude as values reported from measurements on sea-ice at the Arctic Ocean (Persson et al., 2002).

## 5.2 Seasonal differences of the surface energy balance

The surface energy balance at the study site is characterized by a strong seasonality, featuring a distinctly different partitioning of the energy balance within the annual cycle. The seasonal differences in the surface energy balance are caused by factors such as the availability of solar radiation, the surface characteristics and the atmospheric conditions. The differences of these controlling mechanisms are exemplified based on the energy balances during summer and polar winter (Fig. 9).

The radiation budget during the summer season is largely determined by the incoming shortwave radiation, which is further intensified by the polar day conditions. Conversely, the radiation budget during the winter is mainly controlled by thermal radiation facilitated by the high reflectance of the snow cover and the low or not available short wave radiation. In both periods, the surface radiation budget is strongly altered by clouds. Our observations reveal, that the net radiation is attenuated during the summer season by the presence of clouds, while the radiative losses are reduced during winter.

During the summer season, the largest fraction of the net radiation (40–50%) is consumed by the latent heat flux, whereas similar fractions of about 20% are attributed to the sensible and the ground heat flux (Fig. 9). This partitioning of the energy balance is presumably determined by the high soil moisture content at the study site, which controls both the latent heat flux and the ground heat flux. The high soil moisture content at the study site is facilitated by the shallow active layer depth, which also affects the soil temperature gradient and hence the ground heat flux. Consequently, the surface energy balance during the summer time is, to a certain degree, directly affected by the permafrost conditions, in particular by its thermal state and the soil water/ice content. The observed magnitude to the energy balance components corresponds well with values observed at other wet tundra landscapes of similar latitude (Eugster et al., 2000). However, the magnitude of the summer time ground heat flux is at the upper edge of the reported values.

### Permafrost and surface energy balance in Northern Siberia – Part 2

M. Langer et al.

Title Page

Abstract

Introduction

Conclusions

References

Tables

Figures

⏪

⏩

◀

▶

Back

Close

Full Screen / Esc

Printer-friendly Version

Interactive Discussion





**Permafrost and surface energy balance in Northern Siberia – Part 2**

M. Langer et al.

[Title Page](#)[Abstract](#)[Introduction](#)[Conclusions](#)[References](#)[Tables](#)[Figures](#)[⏪](#)[⏩](#)[◀](#)[▶](#)[Back](#)[Close](#)[Full Screen / Esc](#)[Printer-friendly Version](#)[Interactive Discussion](#)

2. The surface energy balance and hence permafrost is very sensitive to the snow cover, especially the timing of snow accumulation and melt, the snow depth and the albedo. Our measurements reveal, that the thermal isolation of the snow cover results in a positive temperature difference of about 4 °C between the average soil and surface temperature. This effect is described in detail in a theoretical study by Goodrich (1982). Due to the high albedo, the surface energy balance during late winter and spring is largely determined by sensible heat flux despite high values of incoming short-wave radiation. Numerous studies demonstrated the impact of the snow cover on the atmospheric conditions ranging from the local scale (meters to kilometers) (e.g. Neumann and Marsh, 1998; Pohl et al., 2006; Bewley et al., 2010) to global effect (e.g. Walland and Simmonds, 1996; Cook et al., 2008).
3. The permafrost at the study site is mainly controlled by the net radiation, which in turn can be strongly altered by clouds, especially during winter. This suggests that the thermal state of permafrost is affected by large scale atmospheric circulation processes such as cyclone activity and the annual dynamics of the Siberian High. The initial warming in spring is mainly forced by sensible heat flux, which additionally suggests a certain contribution of air mass advection to the permafrost heat budget. The impact of atmospheric circulation patterns on the energy balance of the Arctic has been outlined in numerous studies (e.g. Curry et al., 1993; Serreze et al., 2000; Petrone and Rouse, 2000).
4. Our measurements reveal high spatial and temporal variabilities of refreezing. Differences in completion of freeze back between water bodies and soil can amount up to several months and the duration of refreezing in different years can vary up to 3 months. This indicates that the time available for microbial decomposition features a significant spatial and inter-annual variability, which in turn may affect the green house gas emissions especially of small ponds. The importance of high-arctic water bodies for the atmospheric methane budget has been demonstrated by Walter et al. (2006, 2007). These findings have strong implications

for model schemes as introduced by Khvorostyanov et al. (2008), which aim to include biochemical processes in permafrost regions on larger scales.

## 6 Summary and conclusions

Based on the results of the first and the second part of this study, we conclude with an overview of the main characteristics of the annual surface energy balance.

During the entire annual cycle, the surface energy budget is determined by the radiation balance. The net radiation essentially depends on the seasonality of the short-wave radiation budget, the presence or absence of the snow cover and the cloudiness. The snow cover has its greatest impact over 4 months from the end of the polar night until snow melt, when the high snow albedo significantly reduces the net short-wave radiation. Clouds are generally found to reduce the net radiation by about 50% during the snow-free season, while they almost prevent radiative losses during winter.

The turbulent heat fluxes have their largest impact on the surface energy budget during the snow-free period, when they balance about 70% of the net radiation. The latent heat flux is a factor of two higher than the sensible heat flux, so that the average Bowen ratio yields 0.5. During the summer months, the latent heat flux is largely in balance with the observed precipitation rates, which suggests a regionally closed water cycle between the atmosphere and the tundra surface. During the winter period, the latent heat flux is relatively small and so is sublimation at the snow cover. The sensible heat flux reaches its largest relative contribution to the surface energy balance during the late winter period, when it balances almost 70% of the radiative losses. This indicates that warming after the winter period is influenced by the influx of warm air. Furthermore, it is worthwhile to note that the lower atmosphere is well mixed during a major part of the winter season and stable stratifications are very rare.

The ground heat flux is a significant component in the surface energy balance, with relative contributions of about 20% during summer and 60% during polar winter. During the summer months about 60% of the ground heat flux is consumed by active layer

### Permafrost and surface energy balance in Northern Siberia – Part 2

M. Langer et al.

Title Page

Abstract

Introduction

Conclusions

References

Tables

Figures

⏪

⏩

◀

▶

Back

Close

Full Screen / Esc

Printer-friendly Version

Interactive Discussion



thawing, whereas 40% are used for the warming of the soil. The refreezing period, which can last from the end of September until the beginning of December, is mainly controlled by the radiation balance. At that time, clouds and the snow cover have their most persistent impact on the ground thermal regime as they significantly influence the duration of the refreezing period. The rare occurrence of atmospheric inversions near the surface during winter is partly attributed to the considerable ground heat flux. The already high heat storage capacity of the tundra can be further increased by the presence of water bodies, which can be remarkable even for small water bodies, such as ponds.

We conclude that the realistic simulation of the surface energy balance in climate models is mandatory with regard to large scale permafrost predictions. This issue involved the reproduction highly variable features such as cloudiness, snow cover and the thermal soil properties. Furthermore, there are indications that a more accurate representation of the thermal dynamics of permafrost could aid to improve the modeling of the atmospheric boundary layer in the Arctic.

*Acknowledgements.* We are thankful to the Department of Micro-Meteorology of the University of Bayreuth headed by Thomas Foken for providing the eddy-covariance post-processing software. We especially acknowledge the help of Günther Stoof for the support of our field work especially during the spring expeditions. We gratefully acknowledge financial support by the Helmholtz Association through a grant (VH-NG 203) awarded to Julia Boike.

## References

- Beesley, J., Bretherton, C., Jakob, C., Andreas, E., Intrieri, J., and Uttal, T.: A comparison of cloud and boundary layer variables in the ECMWF forecast model with observations at surface heat budget of the Arctic Ocean(SHEBA) ice camp, *J. Geophys. Res.*, 105, 12337–12349, 2000. 1411
- Bewley, D., Essery, R., Pomeroy, J., and Ménard, C.: Measurements and modelling of snowmelt and turbulent heat fluxes over shrub tundra, *Hydrol. Earth Syst. Sci.*, 14, 1331–1340, doi:10.5194/hess-14-1331-2010, 2010. 1412

## Permafrost and surface energy balance in Northern Siberia – Part 2

M. Langer et al.

Title Page

Abstract

Introduction

Conclusions

References

Tables

Figures



Back

Close

Full Screen / Esc

Printer-friendly Version

Interactive Discussion



## Permafrost and surface energy balance in Northern Siberia – Part 2

M. Langer et al.

Title Page

Abstract

Introduction

Conclusions

References

Tables

Figures

◀

▶

◀

▶

Back

Close

Full Screen / Esc

Printer-friendly Version

Interactive Discussion



- Boike, J., Wille, C., and Abnizova, A.: Climatology and summer energy and water balance of polygonal tundra in the Lena River Delta, Siberia, *J. Geophys. Res.-Biogeo.*, 113, G03025, doi:10.1029/2007JG000540, 2008. 1394
- Comiso, J.: Warming trends in the Arctic from clear sky satellite observations, *J. Climate*, 16, 3498–3510, 2003. 1393
- Cook, B., Bonan, G., Levis, S., and Epstein, H.: The thermoinsulation effect of snow cover within a climate model, *Clim. Dynam.*, 31, 107–124, 2008. 1412
- Cox, P., Betts, R., Bunton, C., Essery, R., Rowntree, P., and Smith, J.: The impact of new land surface physics on the GCM simulation of climate and climate sensitivity, *Clim. Dynam.*, 15, 183–203, 1999. 1411
- Curry, J., Schramm, J., and Ebert, E.: Impact of clouds on the surface radiation balance of the Arctic Ocean, *Meteorol. Atmos. Phys.*, 51, 197–217, 1993. 1408, 1412
- Delire, C., Levis, S., Bonan, G., Foley, J., Coe, M., and Vavrus, S.: Comparison of the climate simulated by the CCM3 coupled to two different land-surface models, *Clim. Dynam.*, 19, 657–669, 2002. 1393
- ESA: The Lena River Delta, [http://earth.eo.esa.int/cgi-bin/satimsgsql.pl?show\\_url=1471&startframe=0](http://earth.eo.esa.int/cgi-bin/satimsgsql.pl?show_url=1471&startframe=0), last access: 21 July 2010, 2006. 1423
- Eugster, W., Rouse, W., Pielke Sr., R., McFadden, J., Baldocchi, D., Kittel, T., Chapin, F., Liston, G., Vidale, P., Vaganov, E., and Chambers, S.: Land–atmosphere energy exchange in Arctic tundra and boreal forest: available data and feedbacks to climate, *Global Change Biol.*, 6, 84–115, 2000. 1410
- Foster, J., Sun, C., Walker, J., Kelly, R., Chang, A., Dong, J., and Powell, H.: Quantifying the uncertainty in passive microwave snow water equivalent observations, *Remote Sens. Environ.*, 94, 187–203, 2005. 1400
- Goodrich, L.: The influence of snow cover on the ground thermal regime, *Can. Geotech. J.*, 19, 421–432, 1982. 1412
- Grigoriev, N.: The temperature of permafrost in the Lena Delta Basin – deposit conditions and properties of the permafrost in Yakutia, chap. 2, Yakutsk, 97–101, 1960. 1395
- Hinzman, L., Bettez, N., Bolton, W., Chapin, F., Dyrgerov, M., Fastie, C., Griffith, B., Hollister, R., Hope, A., Huntington, H., et al.: Evidence and implications of recent climate change in Northern Alaska and other arctic regions, *Climatic Change*, 72, 251–298, 2005. 1393
- Høgstrøm, U.: Non-dimensional wind and temperature profiles in the atmospheric surface layer: a re-evaluation, *Bound.-Lay. Meteorol.*, 42, 55–78, 1988. 1397

## Permafrost and surface energy balance in Northern Siberia – Part 2

M. Langer et al.

Title Page

Abstract

Introduction

Conclusions

References

Tables

Figures

⏪

⏩

◀

▶

Back

Close

Full Screen / Esc

Printer-friendly Version

Interactive Discussion



- Holland, M. and Bitz, C.: Polar amplification of climate change in coupled models, *Clim. Dynam.*, 21, 221–232, 2003. 1393
- Johannessen, O., Bengtsson, L., Miles, M., Kuzmina, S., Semenov, V., Alekseev, G., Nagurnyi, A., Zakharov, V., Bobylev, L., Pettersson, L., et al.: Arctic climate change: observed and modelled temperature and sea-ice variability, *Tellus A*, 56, 328–341, 2004. 1393
- Kaplan, J., Bigelow, N., Prentice, I., Harrison, S., Bartlein, P., Christensen, T., Cramer, W., Matveyeva, N., McGuire, A., Murray, D., et al.: Climate change and Arctic ecosystems: 2. Modeling, paleodata-model comparisons, and future projections, *J. Geophys. Res.*, 108, 8171, doi:10.1029/2002JD002559, 2003. 1393
- Kelly, R., Chang, A., Foster, J., and Tedesco, M.: AMSR-E/Aqua 5-day 3 Global Snow Water Equivalent EASE-Grids V002, National Snow and Ice Data Center, Boulder, Colorado, USA, digital media, (data used from 2007–2009), 2004. 1400
- Khvorostyanov, D., Krinner, G., Ciais, P., Heimann, M., and Zimov, S.: Vulnerability of permafrost carbon to global warming, Part I: model description and role of heat generated by organic matter decomposition, *Tellus B*, 60, 250–264, 2008. 1413
- Langer, M., Westermann, S., Muster, S., Piel, K., and Boike, J.: Permafrost and surface energy balance of a polygonal tundra site in northern Siberia - Part 1: Spring to fall, *The Cryosphere Discuss.*, 4, 901–947, doi:10.5194/tcd-4-901-2010, 2010. 1394, 1396, 1397, 1398, 1399, 1400, 1401, 1431
- Lawrence, D. and Slater, A.: A projection of severe near-surface permafrost degradation during the 21st century, *Geophys. Res. Lett.*, 32, L24401, doi:10.1029/2005GL025080, 2005. 1393
- Lawrence, D. and Slater, A.: Incorporating organic soil into a global climate model, *Clim. Dynam.*, 30, 145–160, 2008. 1411
- Lawrence, D., Slater, A., Romanovsky, V., and Nicolsky, D.: Sensitivity of a model projection of near-surface permafrost degradation to soil column depth and representation of soil organic matter, *J. Geophys. Res.*, 113, F02011, doi:10.1029/2007JF000883, 2008. 1393
- Lewkowicz, A.: Evaluation of miniature temperature-loggers to monitor snowpack evolution at mountain permafrost sites, Northwestern Canada, *Permafrost Periglac.*, 19, 323–331, 2008. 1400
- Moritz, R., Bitz, C., and Steig, E.: Dynamics of recent climate change in the Arctic, *Science*, 297, 1497–1502, doi: 10.1126/science.1076522, 2002. 1393
- Neumann, N. and Marsh, P.: Local advection of sensible heat in the snowmelt landscape of Arctic tundra, *Hydrol. Process.*, 12, 1547–1560, 1998. 1412



## Permafrost and surface energy balance in Northern Siberia – Part 2

M. Langer et al.

Title Page

Abstract

Introduction

Conclusions

References

Tables

Figures

◀

▶

◀

▶

Back

Close

Full Screen / Esc

Printer-friendly Version

Interactive Discussion

- Shupe, M. and Intrieri, J.: Cloud radiative forcing of the Arctic surface: the influence of cloud properties, surface albedo, and solar zenith angle, *J. Climate*, 17, 616–628, 2004. 1408
- Stendel, M. and Christensen, J.: Impact of global warming on permafrost conditions in a coupled GCM, *Geophys. Res. Lett.*, 29, 1632, doi:10.1029/2001GL014345, 2002. 1393
- 5 Sturm, M., Holmgren, J., König, M., and Morris, K.: The thermal conductivity of seasonal snow, *J. Glaciol.*, 43, 26–41, 1997. 1399
- Tape, K., Sturm, M., and Racine, C.: The evidence for shrub expansion in Northern Alaska and the Pan-Arctic, *Global Change Biol.*, 12, 686–702, 2006. 1393
- 10 Turner, J., Overland, J., and Walsh, J.: An Arctic and Antarctic perspective on recent climate change, *Int. J. Climatol.*, 27, 277–293, 2007. 1393
- Vavrus, S.: The impact of cloud feedbacks on Arctic climate under greenhouse forcing, *J. Climate*, 17, 603–615, 2004. 1393
- Viterbo, P., Beljaars, A., Mahfouf, J., and Teixeira, J.: The representation of soil moisture freezing and its impact on the stable boundary layer, *Q. J. Roy. Meteor. Soc.*, 125, 2401–2426, 1999. 1393, 1411
- 15 Walland, D. and Simmonds, I.: Sub-grid-scale topography and the simulation of Northern Hemisphere snow cover, *Int. J. Climatol.*, 16, 961–982, 1996. 1412
- Walter, K., Zimov, S., Chanton, J., Verbyla, D., and Chapin, F.: Methane bubbling from Siberian thaw lakes as a positive feedback to climate warming, *Nature*, 443, 71–75, 2006. 1412
- 20 Walter, K., Edwards, M., Grosse, G., Zimov, S., and Chapin III, F.: Thermokarst lakes as a source of atmospheric CH<sub>4</sub> during the last deglaciation, *Science*, 318, 633, 633–636, doi:10.1126/science.1142924, 2007. 1412
- Westermann, S., Lüers, J., Langer, M., Piel, K., and Boike, J.: The annual surface energy budget of a high-arctic permafrost site on Svalbard, Norway, *The Cryosphere*, 3, 245–263, doi:10.5194/tc-3-245-2009, 2009. 1393, 1409
- 25 Zhang, T.: Influence of the seasonal snow cover on the ground thermal regime: an overview, *Rev. Geophys.*, 43, RG4002, doi:10.1029/2004RG000157, 2005. 1399
- Zhang, X., Walsh, J., Zhang, J., Bhatt, U., and Ikeda, M.: Climatology and interannual variability of Arctic cyclone activity: 1948–2002, *J. Climate*, 17(12), 2300–2317, 2004. 1395

**Table 1.** Definitions and constants.

$Q_{\text{net}}$	net radiation
$\Delta Q_{\text{S}}$	net short-wave radiation
$\Delta Q_{\text{L}}$	net long-wave radiation
$Q_{\text{L}\downarrow}$	incoming long-wave radiation
$Q_{\text{HB}}$	buoyancy flux
$Q_{\text{H}}$	sensible heat flux
$Q_{\text{E}}$	latent heat flux
$Q_{\text{G}}$	ground or snow heat flux
$Q_{\text{G,sensible}}$	sensible ground heat flux
$Q_{\text{G,latent}}$	latent ground heat flux
$Q_{\text{net,p}}$	net radiation at the pond
$Q_{\text{G,p}}$	heat flux released from pond
$C$	residual of the energy balance
$u_*$	friction velocity
$\zeta = z/L_*$	stability parameter ( $z$ : measurement height, $L_*$ Obukhov length)
$T_{\text{air}}$	air temperature
$T_{\text{surf}}$	surface temperature
$R_{\text{H}}$	relative humidity
$\theta_w$	volumetric liquid water content
$\theta_{w,\text{min}}$	minimum liquid water content (frozen)
$\theta_{w,\text{max}}$	maximum liquid water content (thawed)
$\theta_i$	volumetric ice content
$P_{\text{dry}}$	porosity
$c_p$	specific heat capacity of air at constant pressure
$\rho_{\text{air}}$	density of air
$\rho_{\text{ice}} = 0.91 \text{ g cm}^{-3}$	density of ice
$\rho_{\text{snow}} = 0.19 \text{ g cm}^{-3}$	density of snow

**Permafrost and surface energy balance in Northern Siberia – Part 2**

M. Langer et al.

Title Page

Abstract Introduction

Conclusions References

Tables Figures

⏪ ⏩

◀ ▶

Back Close

Full Screen / Esc

Printer-friendly Version

Interactive Discussion



## Permafrost and surface energy balance in Northern Siberia – Part 2

M. Langer et al.

**Table 1.** Continued.

$D_h$	thermal diffusivity
$K_h$	thermal conductivity
$C_h$	volumetric heat capacity
$C_{h,i} = 1.9 \text{ MJ m}^{-3} \text{ K}^{-1}$	volumetric heat capacity of ice
$C_{h,s} \approx 2.3 \text{ MJ m}^{-3} \text{ K}^{-1}$	volumetric heat capacity of the solid soil matrix

Title Page

Abstract

Introduction

Conclusions

References

Tables

Figures

⏪

⏩

◀

▶

Back

Close

Full Screen / Esc

Printer-friendly Version

Interactive Discussion

**Permafrost and surface energy balance in Northern Siberia – Part 2**

M. Langer et al.

Discussion Paper | Discussion Paper | Discussion Paper | Discussion Paper | Discussion Paper

**Table 2.** Used soil parameters for ground heat flux calculations during the winter period. Values of porosity  $P_{dry}$  and volumetric ice content  $\theta_i$  are estimated based on soil sample analysis and in situ soil water content measurements during summer. The heat capacities are calculated by weighting  $C_{h,i}$  and  $C_{h,s}$  according to the assumed ice content and porosity. The thermal diffusivities  $D_h$  are determined by using the conductive method described in the first part of this study, from which we evaluate the thermal conductivity values  $K_h$  with the estimated heat capacity. Errors are calculated using Gaussian error propagation.

Substrate	$P_{dry}$	$\theta_i$	$C_h$ (MJ m <sup>-3</sup> K <sup>-1</sup> )	$D_h$ (m <sup>2</sup> s <sup>-1</sup> )	$K_h$ (W m <sup>-1</sup> K <sup>-1</sup> )
Frozen dry peat	0.8±0.1	0.1±0.1	0.7±0.3	0.68±0.19	0.46±0.25
Frozen wet peat	0.8±0.1	0.7±0.1	1.8±0.3	0.54±0.09	0.95±0.23
Frozen saturated peat	0.8±0.1	0.8±0.1	2.0±0.05	0.96±0.09	1.92±0.19
Snow	$\rho_{snow}=190\pm10$ (kg m <sup>-3</sup> )		0.40±0.04	0.54±0.04	0.22±0.03
Ice	$\rho_{ice}=920$ (kg m <sup>-3</sup> )		1.9	1.2	2.3

Title Page

Abstract Introduction

Conclusions References

Tables Figures

⏪ ⏩

◀ ▶

Back Close

Full Screen / Esc

Printer-friendly Version

Interactive Discussion



**Table 3.** Average heat fluxes and essential climate parameters. According to the available dataset, sub-periods are required during the late winter section. Values are in  $\text{W m}^{-2}$ , if not indicated differently. Turbulent heat flux values marked in bold are affected by minor data gaps due to quality assessment or the exclusion of lee wind sectors. Radiation values measured with the NR-Lite sensor are marked with  $^{\ominus}$ , and values obtained with the four component sensor (CNR1) are indicated with  $^{\oplus}$ . Modeled values of latent heat flux are indicated with  $^{\ddagger}$ .

	Early winter		Polar winter		Late winter	
	2007 1 Oct–30 Nov	2008 1 Oct–30 Nov	2007–2008 1 Dec–30 Jan	2008–2009 1 Dec–30 Jan	2008 27 Feb–30 Mar	2009 1 Feb–30 Mar
$Q_{\text{net}}$	-17 $^{\ominus}$	-21 $^{\oplus}$	-21 $^{\ominus}$	-25 $^{\oplus}$	-14.7 $^{\ominus}$	–
$\Delta Q_{\text{S}}$	–	1.5	0	0	–	–
$\Delta Q_{\text{L}}$	–	-22	-21	-25	–	–
$Q_{\text{H}}$	<b>-6</b>	<b>-5</b>	<b>-9</b>	–	<b>-10.3</b>	–
$Q_{\text{E}}$	<b>9<math>^{\ddagger}</math></b>	<b>13<math>^{\ddagger}</math></b>	<b>4<math>^{\ddagger}</math></b>	–	<b>3<math>^{\ddagger}</math></b>	–
$Q_{\text{G}}$	-11	-20	-17	-14	-5.4	-10.4
$Q_{\text{G,sensible}}$	3	-3	-14	-14	-5.4	-10.4
$Q_{\text{G,latent}}$	-14	-17	-3	0	0	–
$C$	-9	-9	-1	–	2	–
$Q_{\text{net,p}}$	-18	-23	-22	-25	-20	-21.5
$Q_{\text{G,p}}$	-12 $^{\ddagger}$	-34 $^{\ddagger}$	-32	-28	-12.6	-22.3
$T_{\text{surf}}$ ( $^{\circ}\text{C}$ )	-16	-15	-29.9	-29.7	-25.9	-35.5
$T_{\text{air}}$ ( $^{\circ}\text{C}$ )	-16.1	-14.8	-29.7	-29.5	-24.8	-34.7
$R_{\text{H}}$ (%)	81	–	70	–	75	–
Snow depth (m)	0.09	0.05	0.11	0.15	0.18	–

## Permafrost and surface energy balance in Northern Siberia – Part 2

M. Langer et al.

Title Page

Abstract

Introduction

Conclusions

References

Tables

Figures

◀

▶

◀

▶

Back

Close

Full Screen / Esc

Printer-friendly Version

Interactive Discussion



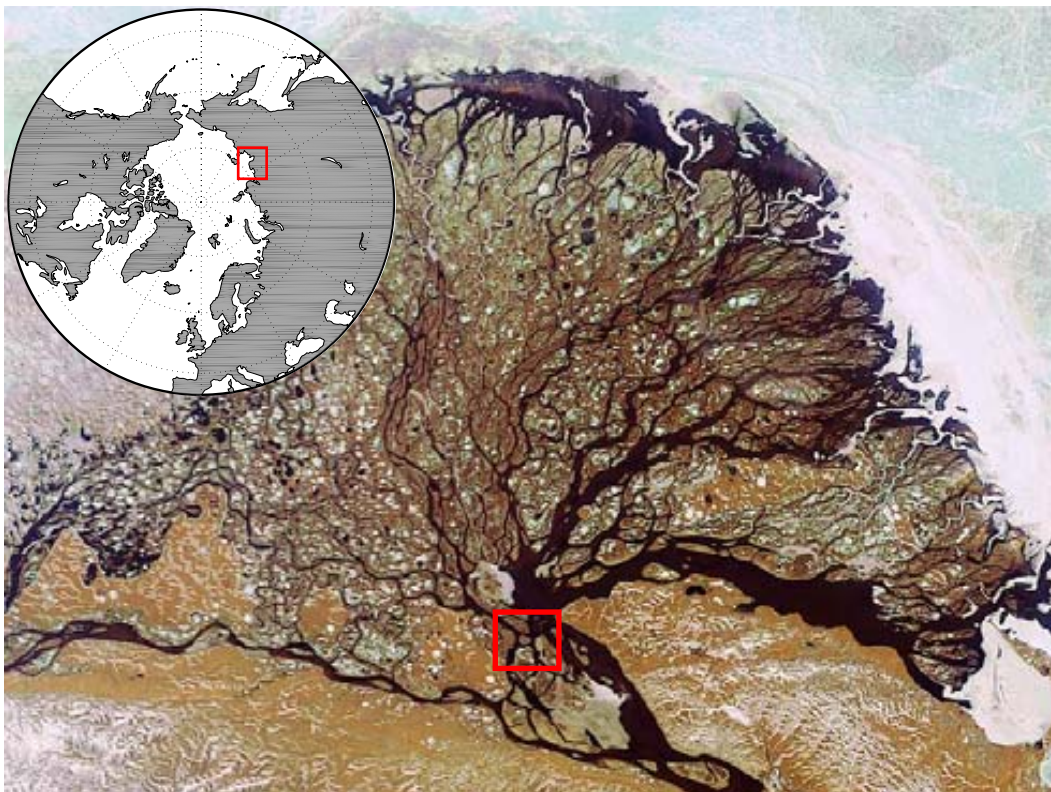


**Fig. 1.** The location of the study site in the Lena River Delta on a Envisat (MERIS) image acquired on 15 June 2006 (ESA, 2000). The Lena Delta covers an area of approximately 30 000 km<sup>2</sup>.

**Permafrost and surface energy balance in Northern Siberia – Part 2**

M. Langer et al.

Title Page

Abstract

Introduction

Conclusions

References

Tables

Figures

⏪

⏩

◀

▶

Back

Close

Full Screen / Esc

Printer-friendly Version

Interactive Discussion



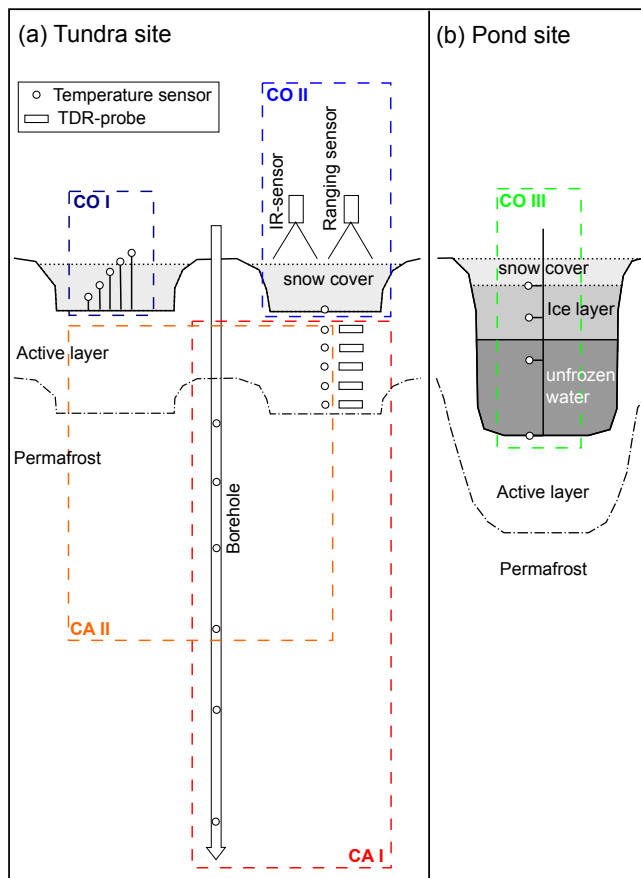


**Fig. 2.** Scheme of the different measurement setups used for the evaluation of subsurface heat flux. **(a)** Cross-section of the tundra soil indicating polygonal rims and centers. **(b)** Cross-section of the polygonal pond during the stage of freezing. Note that, the depicted scheme is not to scale.

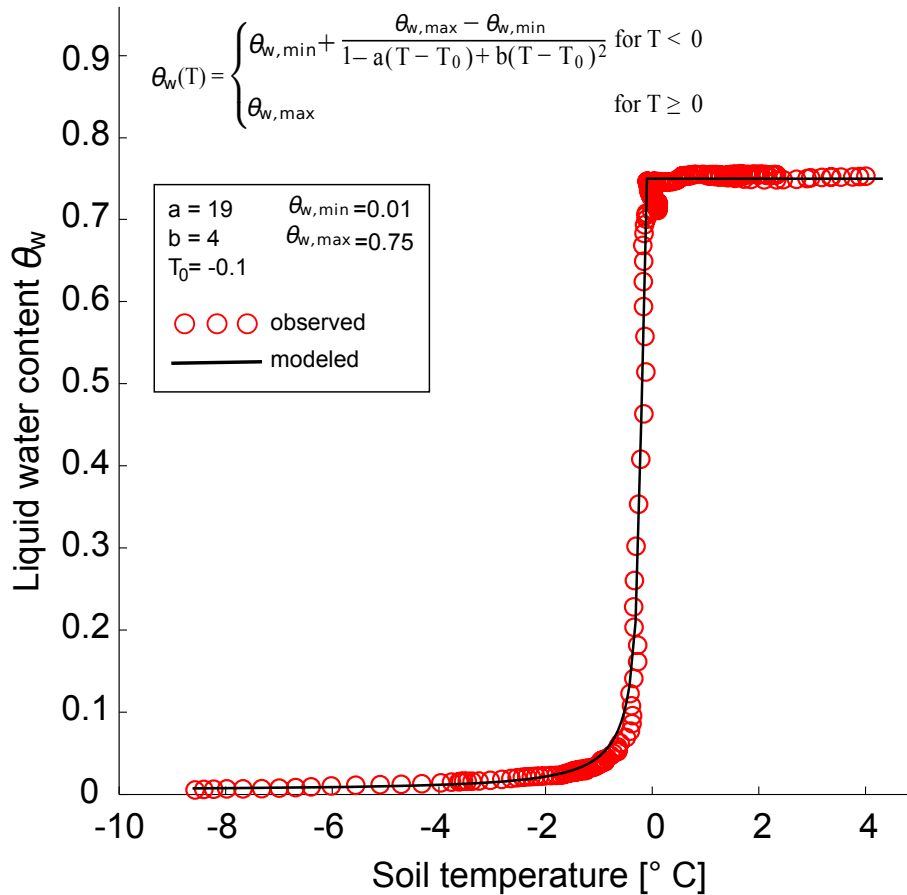


**Fig. 3.** The freezing characteristic of the soil at the study site, which parameterizes the soil water content  $\theta_w$  in dependence to the soil temperature. The used polynomial function and the fitted parameters are depicted in the figure.

**Permafrost and surface energy balance in Northern Siberia – Part 2**

M. Langer et al.

[Title Page](#)

[Abstract](#)    [Introduction](#)

[Conclusions](#)    [References](#)

[Tables](#)    [Figures](#)

[◀](#)    [▶](#)

[◀](#)    [▶](#)

[Back](#)    [Close](#)

[Full Screen / Esc](#)

[Printer-friendly Version](#)

[Interactive Discussion](#)



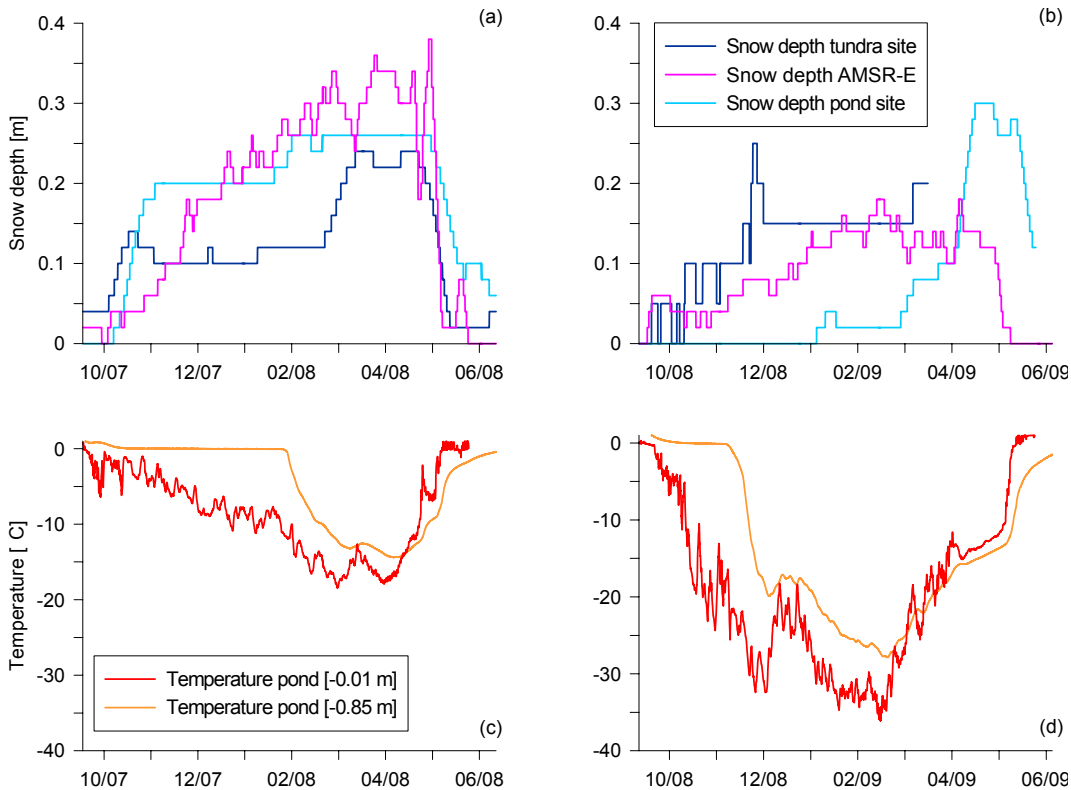


**Fig. 4.** The diagrams at the top show the evolution of the snow depth measured at the tundra site (polygonal center) and the pond site during the winter periods of **(a)** 2007 and **(b)** 2008. Moreover, we depict the snow depth inferred from the AMSR-E snow-water equivalent product using a snow density of  $190 \text{ kg m}^{-3}$  for both periods. The diagrams at the bottom depict the temperatures observed at the surface and the top of sediment of the investigated polygonal pond for the winter periods of **(c)** 2007 and **(d)** 2008.

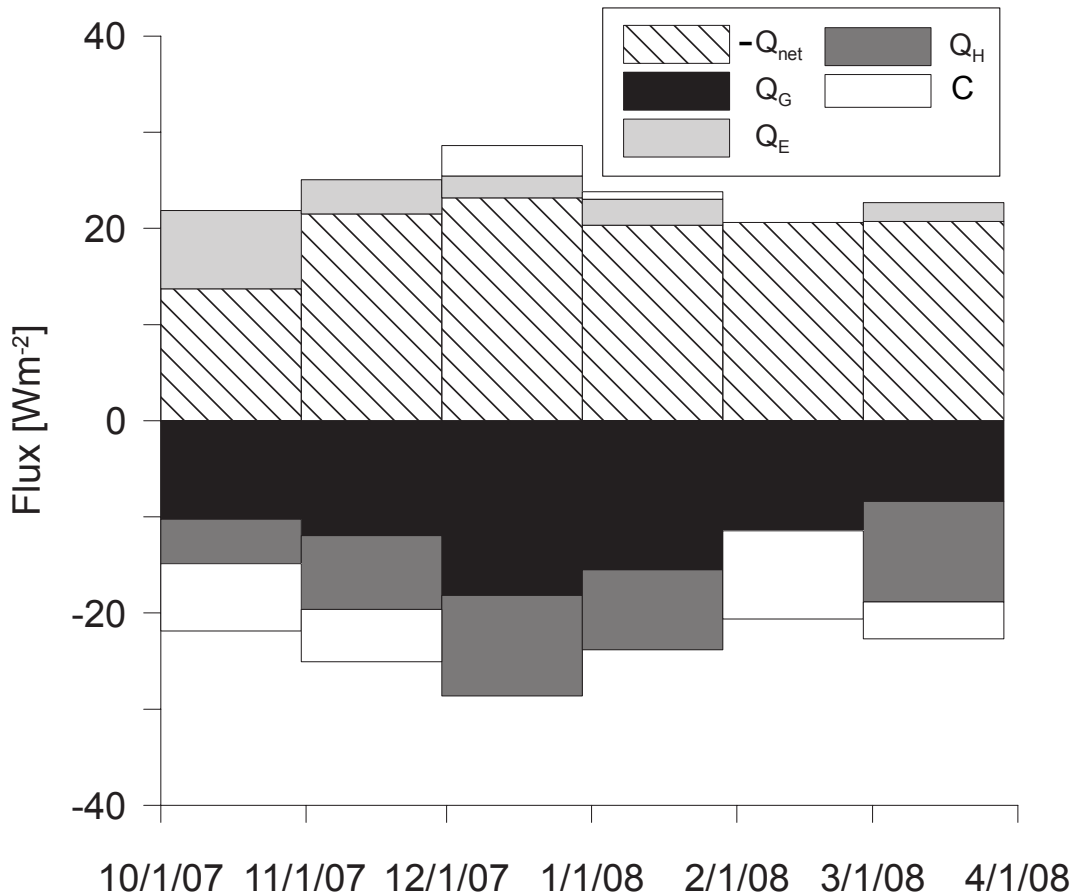


**Fig. 5.** Monthly averages of energy balance components for the winter 2007/2008. Note that the net radiation  $Q_{\text{net}}$  is depicted with opposite sign.

**Permafrost and surface energy balance in Northern Siberia – Part 2**

M. Langer et al.

Title Page

Abstract Introduction

Conclusions References

Tables Figures

⏪ ⏩

◀ ▶

Back Close

Full Screen / Esc

Printer-friendly Version

Interactive Discussion



## Permafrost and surface energy balance in Northern Siberia – Part 2

M. Langer et al.

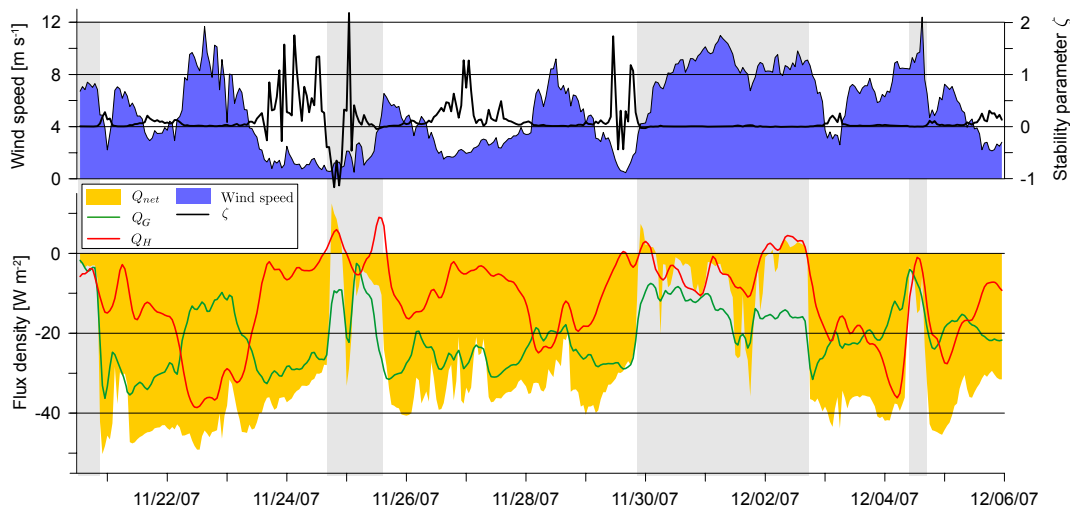


**Fig. 6.** Exemplary measurements of  $Q_{\text{net}}$ ,  $Q_{\text{H}}$  and  $Q_{\text{G}}$  during the transition from early to polar winter in 2007 (lower graph). Presumably overcast conditions are shaded. Measurements of the wind speed and the stability parameter  $\zeta$  are depicted in the upper graph.

[Title Page](#)
[Abstract](#)
[Introduction](#)
[Conclusions](#)
[References](#)
[Tables](#)
[Figures](#)
[◀](#)
[▶](#)
[◀](#)
[▶](#)
[Back](#)
[Close](#)
[Full Screen / Esc](#)
[Printer-friendly Version](#)
[Interactive Discussion](#)

**Permafrost and  
surface energy  
balance in Northern  
Siberia – Part 2**

M. Langer et al.

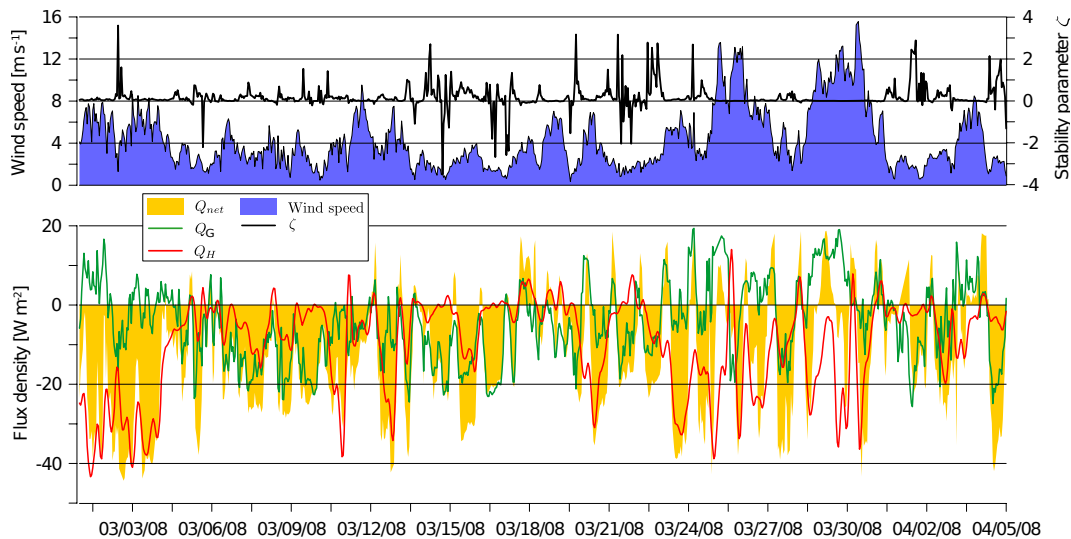


**Fig. 7.** Measurements of  $Q_{net}$ ,  $Q_H$  and  $Q_G$  during the late winter in 2008 (lower graph). The wind speed and the stability parameter  $\zeta$  are depicted in the upper graph.

Title Page

Abstract

Introduction

Conclusions

References

Tables

Figures

◀

▶

◀

▶

Back

Close

Full Screen / Esc

Printer-friendly Version

Interactive Discussion

**Permafrost and surface energy balance in Northern Siberia – Part 2**

M. Langer et al.

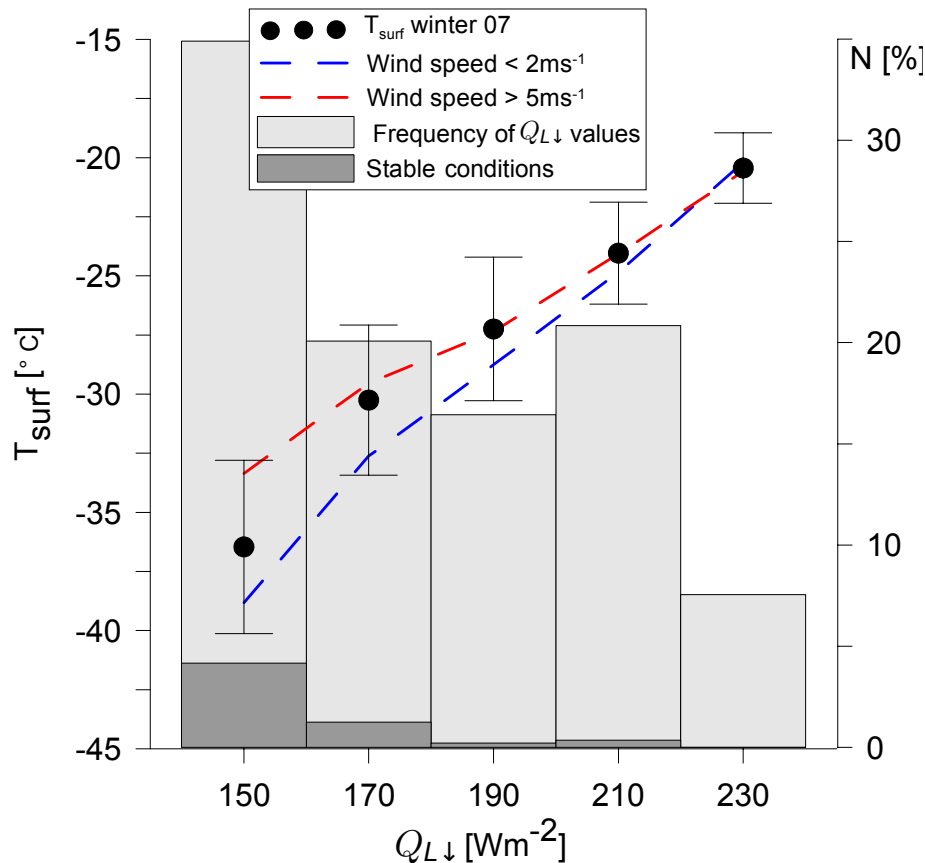


**Fig. 8.** The surface temperature  $T_{\text{surf}}$  in dependence to the incoming long-wave radiation  $Q_{L\downarrow}$  and different wind speeds. The first histogram (light grey) indicates the frequency of observations that feature the displayed classes of incoming long-wave radiation. The second histogram (dark grey) shows the occurrence of stable atmospheric stratification under the different  $Q_{L\downarrow}$  conditions.

Title Page

Abstract

Introduction

Conclusions

References

Tables

Figures

◀

▶

◀

▶

Back

Close

Full Screen / Esc

Printer-friendly Version

Interactive Discussion

Permafrost and surface energy balance in Northern Siberia – Part 2

M. Langer et al.

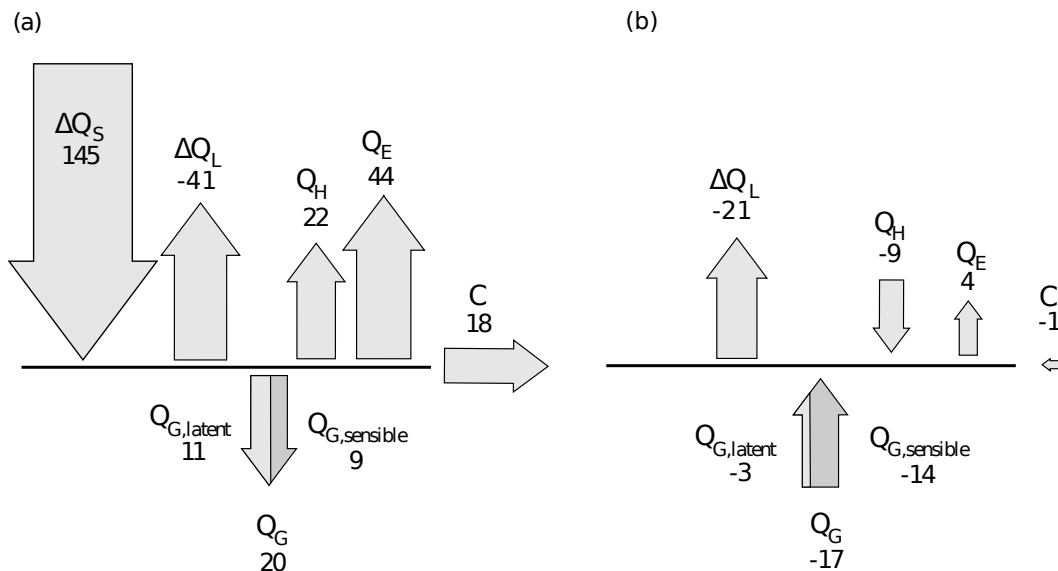


**Fig. 9.** The partitioning of the surface energy balance during **(a)** the summer period from 7 June–30 August 2008 (compare Langer et al., 2010) and **(b)** the winter period from 1 December 2007–30 January 2008 (Table 6). The areas of the arrows are scaled according to the heat flux values. The subsurface heat flux at the tundra site  $Q_G$  is separated according to the energy storage of sensible  $Q_{G,sensible}$  and latent heat  $Q_{G,latent}$ .

Title Page

Abstract Introduction

Conclusions References

Tables Figures

⏪ ⏩

◀ ▶

Back Close

Full Screen / Esc

Printer-friendly Version

Interactive Discussion

